

USING GRANULAR BEDFORMS AND BEDROCK LANDFORMS TO CHARACTERIZE THE AEOLIAN ENVIRONMENT AT OXIA PLANUM, MARS. E.A. Favaro¹, M.R. Balme¹, J. Davis², P.M. Grindrod², P. Fawdon¹, J.D. McNeil¹, A.M. Barrett¹, S.R. Lewis¹, School of Physical Sciences, Open University, Walton Hall, Milton Keynes MK7 6AA, UK (elena.favaro@open.ac.uk), Department of Earth Sciences, Natural History Museum, London, UK.

Introduction: The European Space Agency's ExoMars Rosalind Franklin Rover will land at Oxia Planum (OP) in 2023 [1]. The rover's main mission is to search for biosignatures preserved in the aqueously altered Noachian (>3.7 Ga) phyllosilicate-rich terrain of the landing site [1-3]. In order to safely navigate to potential drill sites, a comprehensive understanding of the aeolian-altered terrain is needed.

Methods: We used multiple methods of data acquisition and analysis to characterize the aeolian-dominated landscape and plaeo- and contemporary wind regimes of the Oxia Planum region. First, machine learning, manual mapping, and change detection techniques were used to identify, map, and determine the migration, morphometrics, distribution, and orientations of transverse aeolian ridges (TARs) and periodic bedrock ridges (PBRs), as well as dust devils, dust devil tracks, and windstreaks in HiRISE images in and around the 1-sigma landing ellipses (Site A in Figure 1). Then, we used Global Circulation Model (GCM) near surface winds derived from several contemporary re-analyses of spacecraft thermal and dust opacity data [4] to obtain the best possible understanding of the current wind regime at OP.

Observations: *Transverse Aeolian Ridges:* With the help of the NOAH-H (NOvelty and Anomaly Hunter – HiRISE) machine learning system [5], we identified, digitized, and measured the along-crestline lengths and orientations of 10,753 TARs in study site A (Figure 1). Irrespective of sun angle in HiRISE images, TARs exhibited an albedo difference on either side of their crest. Using the established grainsize-albedo relationship of stoss and lee slopes observed in terrestrial megaripples [6], we interpreted formative winds necessary for TAR orientation originated from the NW-NNW and blew towards the SE-SSE. Using NOAH-H and manual mapping techniques, we were also able to ascribe a percent-coverage value to 1 km² quadrants across the landing ellipses [7], noting where hazardous traversability conditions could impact rover operations.

Periodic Bedrock Ridges: PBRs were found to be a ubiquitous feature across the OP region, and especially in the south-east of the landing ellipses. In study site A (Figure 1), we mapped 457 PBRs, noting their size and crestline orientation. Because PBRs develop perpendicular to unidirectional winds, we determined a

N-NNE or S-SSW (180° ambiguity) would be responsible for their expression on the landscape.

We recognized a relationship between PBRs and Fe/Mg-rich phyllosilicate terrain (hydrous clay-bearing units; [1]) around the landing site and extended our catalogue of PBRs to include the wider OP region (Site B in Figure 1). Using an observational matrix made up of a ~10x10 km² gridded system, we mapped the distribution and orientation of assemblages of PBRs in HiRISE, CTX, and CaSSIS images. We found that 63% of mapped PBRs were found on clay-bearing terrain – a percentage overlap much higher than would be expected if the phenomena were random. It remains to be seen whether these clay-bearing units are more amenable to abrasion or are more adept at retaining landscape-level signals of wind than non-clay-bearing units.

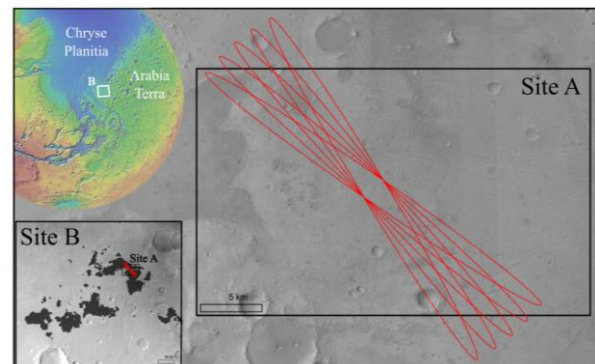


Figure 1. (Top inset) Location of Oxia Planum in relation to Chryse Planitia and Arabia Terra. Site A is the extent in which TARs and PBRs were first mapped. Red ellipses are the landing ellipses as they were calculated in 2020. (Bottom inset) Site B shows the extent of the hydrous clay detections [1] and is the total extent to which PBRs were mapped.

Dust Devils, Dust Devil Tracks, and Windstreaks: HRSC and CaSSIS images were used to identify and track 6 active dust devils in OP [8], while change between consecutive CTX images (captured 50 Earth days apart) identified 649 dust devil tracks or windstreaks. These features exhibited two orientations: a dominant WNW-ESE (180° ambiguity) direction, and a secondary NNE-SSW (180° ambiguity) direction. These directions are in line with the movement of two active dust devils.

Climate Modelling: We compared the GCM winds from the reanalysis at 1.5 m above the surface at OP for MY 24, 25 (global dust event year), 26, and 33 (no dust

events). GCM predictions for all four years show variable directionality and speeds. Wind speeds did not exceed 21 ms^{-1} [3], with 50th %ile winds between $3\text{--}7 \text{ ms}^{-1}$. An analysis of seasonality (at $L_s=0/360, 90, 180, 270$) is typified by variability in wind speed and direction that cannot account for the orientations of TARs or PBRs. Similarly, varying obliquities (low [$5^\circ/15^\circ$], current [25°], and high [$35^\circ/45^\circ$]) in MY 24 for the entire record, and for only the strongest 5% of wind speeds, could not account for the orientation of TARs, but could, in a few cases, account for the orientation of PBRs.

Conclusions: This work was the first to comprehensively evaluate the aeolian environment at OP using granular bedform, bedrock landforms, inferred near-surface winds, and GCMs. Based on landscape-level observations and GCM analyses, we identified multiple wind epochs at OP:

1. The oldest winds, which blew from the N-NNE or S-SSW (180° ambiguity) are recorded in the crestline orientation of PBRs.
2. Winds responsible for the orientation of TARs originated in the NW-NNW and blew towards the SE-SSE. Interestingly, the orientation of the slip faces and horns of barchanoid dunes in craters northeast and southeast of OP [8,9] agree with this wind direction.
3. Contemporary winds or contemporary gusts, realized by the directionality of active dust devils and dust devil tracks, is primarily oriented in a WNW-ESE direction (180° ambiguity), with a secondary orientation from NNE-SSW (180° ambiguity).

Acknowledgments: We gratefully acknowledge support from the UK Space Agency and the European Space Agency. The standard data products used here are available from the NASA PDS (<https://pds.jpl.nasa.gov/>) and ESA PDS (<https://archives.esac.esa.int/psa>). CaSSIS is a project of the University of Bern funded through the Swiss Space Office via ESA's PRODEX program. The instrument hardware development was also supported by the Italian Space Agency (ASI) (ASI-INAF agreement no. I/018/12/0), INAF/Astronomical Observatory of Padova, and the Space Research.

References: [1] Carter et al. (2015), *46th LPSC, No. 1988*. [2] Quantin-Nash et al. (2021), *Astrobiology*, 21(3). [3] Mandon et al. (2021), *Astrobiology*, 21(4). [4] Holmes et al. (2020), *Planet Space Sci*, 104962. [5] Barrett et al. (2022), *Icarus*, 371 (114701) [6] Favaro et al. (2020), *Icarus*, 346. [7] Fawdon et al. (2022), *Journal of Maps*, 17(2). [8] Favaro et al. (2021), *JGR:*

Planets, 126 (e2020JE006723). [9] Chojnacki et al. (2019), *Geology*, 47(5).